Alternately layered Au/Fe_3O_4 with porous structure—a self-assembled nanoarchitecture for catalysis materials†

Satoshi Kameoka*[a] and An-Pang Tsai[ab]

Received 2nd June 2010, Accepted 6th July 2010
DOI: 10.1039/c0jm01708f

Nanoporous gold fabricated by the dealloying of binary Au alloys has a three-dimensional network of fine ligaments on the nano-scale, which is a novel unsupported gold catalyst with exceptional catalytic activity for CO oxidation. Here we report a new nanoporous structure—a composite formed by alternately layered Au/Fe_3O_4/Au with layer spacing ~200 nm and with porous structure (the pore size is below 20 nm). The Au/Fe_3O_4/Au revealed much higher catalytic performance for CO oxidation than the previously reported conventional Au/Fe_2O_3 catalyst, where the porous Au and porous Fe_3O_4 were responsible for the high activity and high thermal stability, respectively. The porous structure is formed *via* a self-assembly process by the dealloying of Al in a NaOH aqueous solution for a conventionally melting Al-Au-Fe alloy precursor with an alternately layered Al_2Au/Al_2Fe/Al_2Au structure. We show here, that a fine composite nanoporous structure could be intentionally designed on the basis of the metallurgically tailored microstructure of the precursor alloy.

Porous metals have been attracting attention as useful functional materials, for example, as catalysts, sensors and in electrochemical devices.[1,2] In particular, RANEY®-type catalysts with a porous structure are widely used as heterogeneous catalysts with excellent performance characteristics for liquid-phase and gas-phase reactions.[3] In general, RANEY®-type catalysts are formed by the leaching of aluminum from Al–TM alloys (TM = Ni, Cu, Co) with an alkaline aqueous solution. However, in many cases there are problems associated with thermal stability and handling of these materials that have limited the utilization of these catalysts.

Recently, a dealloying process using the selective dissolution of elements with varying electrochemical activities has been used to fabricate nano- or mesoporous metals.[4–7] A typical example is the dealloying of Ag from Ag-Au alloys to form nanoporous Au.[7–9] Nanoporous Au has been verified by electron beam tomography method to have a three-dimensionally porous structure on the nano-scale.[10] It was also revealed to have extraordinarily high activity for CO oxidation even at low temperatures.[8,9,11] Since Au and Ag form a solid solution over the whole compositional range the atomic sites for each atom in the alloy are not well defined. This creates a difficulty in determining treatment conditions with the change in composition. Independent of the Au-Ag system, selective dissolution (leaching) of Cu from an intermetallic Cu_3Au compound was found to create homogeneous mesoporous Au.[12] An intermetallic compound, in which atoms are located at definite positions in an orderly manner, generally has a sharp stoichiometric composition. This characteristic ensures homogeneity on the atomic level, different from a solid solution wherein atoms are located randomly at lattice points. In spite of the small surface area (~ 1 m^2/g) the mesoporous Au exhibited high activity, comparable to standard Au/TiO_2 for CO oxidation.[12] This implies that the nano-sized Au and oxide supports may not be the only causes for the high activity, and suggests that mesoporous Au has the potential of being an unsupported catalyst. This demonstrates that an intermetallic compound is a promising precursor for leaching for the fabrication of a nano-architecture and for obtaining unsupported catalysts.

Unsupported porous metallic catalysts are very promising materials since the microstructure and composition of the alloys are easily controlled. Naturally, one would expect to extend an unsupported catalyst with composite dual porous metals exhibiting multiple functions. The composite porous metals could improve the catalytic activity or create a new catalytic function, and could enhance thermal stability, depending on the combination of metals. The resultant porous structure is determined by the microstructure of the precursor alloys. Therefore, in terms of microstructure-tailoring for an expected composite porous structure, metallurgical knowledge and processes are indispensable. For example, unsupported porous metal catalysts such as nanoporous Au are generally unstable at high temperatures.[9,13,14] This could be overcome by developing a designed dual porous structure adjoining each other, one for the high heat resistance phase and/or the other for high catalytic activity. Such a dual porous structure is likely to impart high thermal stability as well as the dual catalytic functionality. In metallurgy, the microstructure of the precursor alloy tailored for the dual porous structure is readily obtained through eutectic solidification wherein a melt is solidified to two solid phases at eutectic composition and eutectic temperature. In this study, we designed a fine lamellar structure formed by intermetallic compounds Al_2Au and Al_2Fe alternately in a conventionally solidified $Al_{67}Au_{19}Fe_{14}$ alloy. After dealloying by leaching with a NaOH aqueous solution, the microstructure was replaced by an alternately layered Au/Fe_3O_4/Au dually-porous composite structure exhibiting extremely high activity for CO oxidation and high thermal stability.

Alloys with compositions of $Al_{67}Au_{19}Fe_{14}$, Al_2Au and Al_2Fe were prepared from the pure elements with a purity of 99.9 wt.% in an arc

[a]*Institute of Multidisciplinary Research for Advanced Materials (IMRAM), Tohoku University, 2-1-1 Katahira, Aoba-ku, Sendai, 980-8577, Japan. E-mail: kameoka@tagen.tohoku.ac.jp; Fax: +81-22-217-5404; Tel: +81-22-217-5723*
[b]*National Institute of Materials Science (NIMS), 1-2-1 Sengen, Tsukuba, 305-0047, Japan*

† Electronic supplementary information (ESI) available: Arrhenius plots for the reaction rate of CO oxidation over porous Au (Al-Au), nanoporous Au/Fe_3O_4/Au (Al-Au-Fe), Fe_3O_4 particles (Al-Fe) and reference Au/Fe_2O_3 catalysts using the data in Fig. 3(a). The high-resolution SEM images of the leached Al-Au-Fe alloy showing the interface between the non-leached and the leached regions. See DOI: 10.1039/c0jm01708f

furnace in an Ar atmosphere. Hereafter, alloy samples of $Al_{67}Au_{19}Fe_{14}$, Al_2Au and Al_2Fe are called Al-Au-Fe, Al-Au and Al-Fe, respectively. The alloy samples were crushed to powder form with particle sizes of interest (< 200 μm) in a ball mill. The surface area of the particles was determined by BET analysis. The sample powders were leached in a 10 wt.% NaOH aqueous solution, kept in the aqueous solution for 4 h at room temperature, and then filtered and thoroughly washed with distilled water until no alkali was detected in the filtrate. The X-ray powder diffraction data were collected using the beam line 15XU (λ = 0.65297 Å) at the SPring-8 facility in Japan.[15] The morphology and microstructure of the sample were observed with a field-emission scanning electron microscope (JEOL JSM-6500F and/or Zeiss Gemini ULTRA-55) equipped with a dispersive X-ray analyzer (JEOL Ex-23000BU) and a transmission electron microscope (JEOL 2010). The reaction was carried out in a standard fixed-bed flow reactor by passing a gaseous mixture of CO (4 vol. %) and O_2 (2 vol. %) in a He flow at a total flow rate of 50 cm^3 min^{-1} over 50 mg of the catalyst (total pressure: 1 atm; space velocity (SV): 120 000 h^{-1}). All the catalysis experiments were performed on fresh materials without any pretreatment. The products were monitored by an on-line gas chromatograph (Shimadzu GC-8A) equipped with molecular sieves 5Å (O_2, CO) and Porapak Q (CO_2). The catalytic activity for the oxidation of CO with O_2 was evaluated by the percentage conversion of CO to CO_2. The data in the catalytic initial activity measurements were recorded after 30 min when the reaction temperature was reached for each temperature setting.

Fig. 1 shows the microstructure of Al-Au-Fe prepared by a conventional arc melting method. The powder XRD pattern in Fig. 1 (a) shows that the diffraction pattern for Al-Au-Fe is almost identical to that for the Al_2Au phase, except for an extra peak appearing around 18° which corresponds to the strongest peak of the Al_2Fe phase. Due to the much smaller scattering power of Al_2Fe compared to Al_2Au, the diffraction peaks of Al_2Fe are relatively weak and some of them are even invisible. Fig. 1 (b) is an SEM image of a typical lamellar structure of Al-Au-Fe, wherein a multilayer-like structure is observed. EDS elemental mapping was employed to distinguish between Al_2Au and Al_2Fe. Fig. 1 (c) shows the element mapping for Au, Fe and Al. It is clear that the contrast from Au is segregated at the layer where the contrast from Fe is significantly weaker, indicating that Au is also immiscible with Fe. These results prove chemically that the lamellar structure of the Al-Au-Fe alloy is composed of the alternately layered $Al_2Au/Al_2Fe/Al_2Au$ with interlamellar spacing around 200 nm. Considering the immiscibility between Au and Fe, and the absence of the formation of a ternary compound in the ternary Al-Au-Fe system, we conclude that the lamellar structure is formed by alternate layers of Al_2Au and Al_2Fe *via* eutectic solidification at a composition close to $Al_{67}Au_{19}Fe_{14}$. Surprisingly, the interlamellar spacing of Al-Au-Fe is more than one order of magnitude smaller than that of the conventional eutectic structure. It should be noted that the interlamellar spacing of lamellar structures is generally under 10 μm depending on the growth conditions.[16]

Fig. 2 shows the high-resolution powder X-ray diffraction patterns (a) and an SEM image (b) for the same alloy as in Fig. 1 but after leaching. The lamellar structure with sharp interfaces is still clearly preserved in the leached Al-Au-Fe alloy. After leaching, XRD of the binary Al-Fe and Al-Au alloys shows diffraction peaks of Fe_3O_4 and fcc-Au, respectively. Owing to the relatively poor scattering power of Fe_3O_4, only diffraction peaks of fcc-Au are detected in the leached Al-Au-Fe. Obviously, the lamellar structure in Fig. 2 (b) is formed by the alternate layers of Fe_3O_4 and Au. This reconfirms that even before leaching, the Au and Fe were completely separated into two different regions in the Al-Au-Fe alloy. The phase diagram of binary Au-Fe indicates an immiscible system wherein the two elements show neither solubility nor the formation of any intermetallic compound.[17] The microstructures in Fig. 1 and Fig. 2 reveal that Al_2Au and Al_2Fe completely phase separate upon solidification, and support the idea that this immiscibility probably exists in the pseudo-binary Al_2Au-Al_2Fe system. The brighter contrast regions are porous Au and the darker ones are nanoparticles of Fe_3O_4 (Fig. 2 (c)). The high-resolution TEM image in Fig. 2 (d) for the cross-section of the alternating $Au/Fe_3O_4/Au$ layered structure verifies that the Au regions have a porous structure with an average pore size of ~5 nm, and that the Fe_3O_4 regions are aggregates of nanoparticles with an average size of ~20 nm. In the binary system, we also verified that the leached Al-Au is an Au porous structure whereas the leached Al-Fe results in

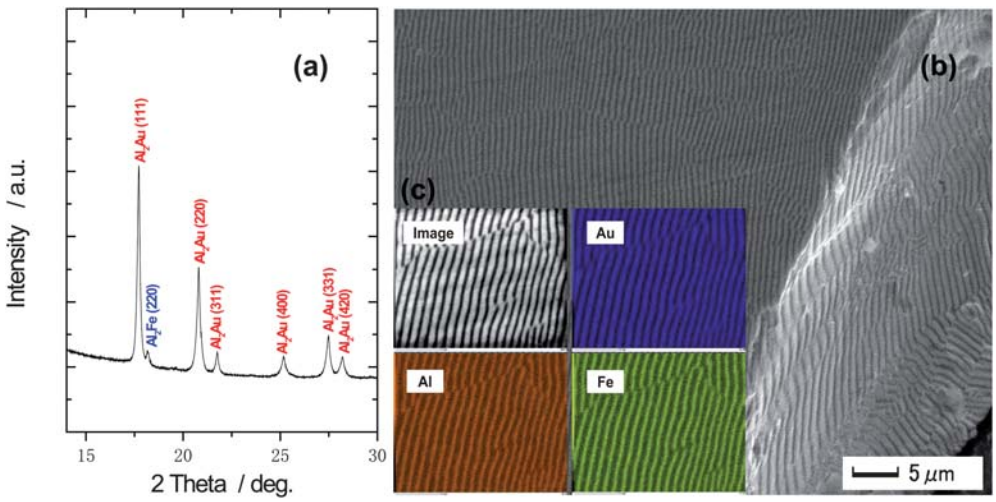

Fig. 1 Powder X-ray diffraction patterns (a) scanning electron micrograph (b) and EDS elemental mapping (c) of a conventionally solidified Al-Au-Fe ($Al_{67}Au_{19}Fe_{14}$).

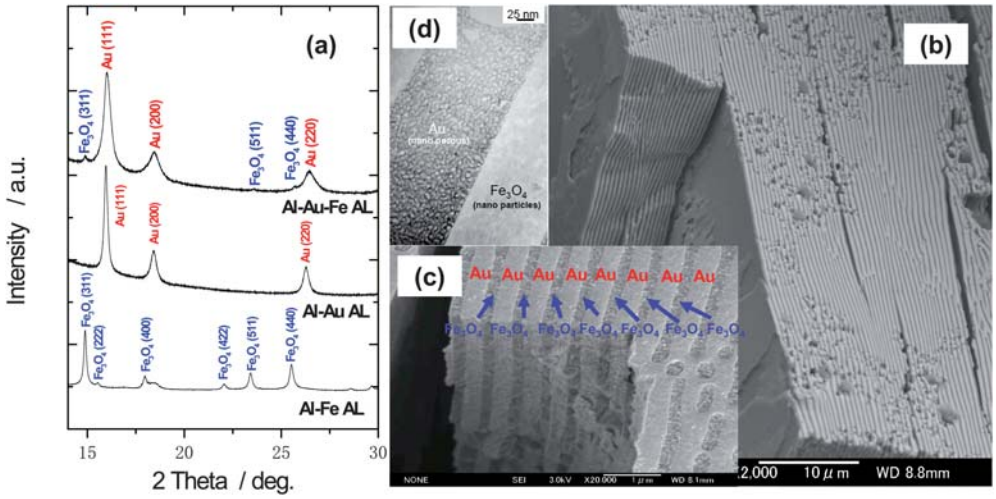

Fig. 2 Powder X-ray diffraction pattern (a) high-resolution scanning electron micrograph (b, c) and high resolution TEM image (d) for the Al-Au-Fe after leaching with an NaOH aqueous solution. Powder X-ray diffraction patterns of leached Al-Fe and leached Al-Au are also shown for comparison.

Table 1 Results of composition (at.%), dissolution of Al (%), BET surface area ($m^2\ g^{-1}$) and reaction rate of CO oxidation for different alloys after leaching

		Composition (at.%)[a]						Dissolved Al	S_{BET}	Reaction rate[b]	
		Before leaching			After leaching						
Sample	Phase	Al	Au	Fe	Al	Au	Fe	(%)	($m^2\ g^{-1}$)	(mmol $min^{-1}\ g^{-1}$ -cat)	(μmol $min^{-1}\ m^{-2}$ -cat)
Al-Au	Al_2Au	66.7	33.3	—	0.6	99.6	—	99.7	5.0	0.14	28.9
Al-Au-Fe	$Al_2Au + Al_2Fe$	67.0	19.0	14.0	3.4	57.9	38.7	98.3	20.2	0.46	22.5
Al-Fe	Al_2Fe	66.7	—	33.3	12.0	—	88.0	93.2	24.5	<0.01	<0.1
Au/Fe_2O_3[c]	$Au + Fe_2O_3$	—	—	—	—	—	—	—	33.9	0.13	3.8

[a] Estimation from ICP analysis. [b] Reaction rates estimated from the data in Fig. 3 (a); CO oxidation at 293K under CO (4%)+O_2 (2%) on 50 ml/min. [c] Loading of Au is 4.4 wt.%; average Au particle size is *ca.* 3.6 nm (by TEM); supplied by World Gold Council (ref. 21).

aggregates of nano-Fe_3O_4 particles. Clearly, these characteristics of the microstructure are still preserved in the Al-Au-Fe alloy even after dealloying. The results of the composition change and dissolution of Al (%) after the leaching treatment are given in Table 1. Most of the Al will be dissolved into solution and consequently Au and Fe skeletons are left behind. The residual Al in the leached Al-Au-Fe mainly exists in the Al-Fe phase. There have been a large number reports on artificial multilayered structures of metal/oxide prepared by sputtering or MBE methods,[18–20] however, in all of these cases, each metal or oxide layer was shown to have a dense structure. To the best of our knowledge, the alternately layered metal/oxide porous nano-composite reported in this study is the first example of such a structure.

Fig. 3 (a) shows the CO conversion as a function of reaction temperature for the CO oxidation over the leached Al-Au-Fe, Al-Au and Al-Fe alloys. To compare their catalytic initial activities under the same reaction conditions with that of a previously reported good catalyst, we employed a sample of 5% Au/Fe_2O_3 (TYPE C; Lot No #02-5) supplied by the World Gold Council.[21] The leached Al-Au-Fe, *i.e.*, the resultant $Au/Fe_3O_4/Au$ nanoporous structure, reveals a much higher initial activity than all the other catalysts. Although the Fe_3O_4 prepared from dealloying of Al-Fe is itself not active for the CO oxidation reaction in this temperature range, the initial activity of the $Au/Fe_3O_4/Au$ nanoporous structure is much higher than that of the Au porous structure prepared from dealloying Al-Au (Fig. 3 (a)). According to the estimation from the Arrhenius plots for the CO oxidation (Fig. S1, ESI†), the apparent activation energy of the nanoporous $Au/Fe_3O_4/Au$ (35.8 kJ mol^{-1}) is very close to that of the reference Au/Fe_2O_3 (34.1 kJ mol^{-1}). The values of these activation

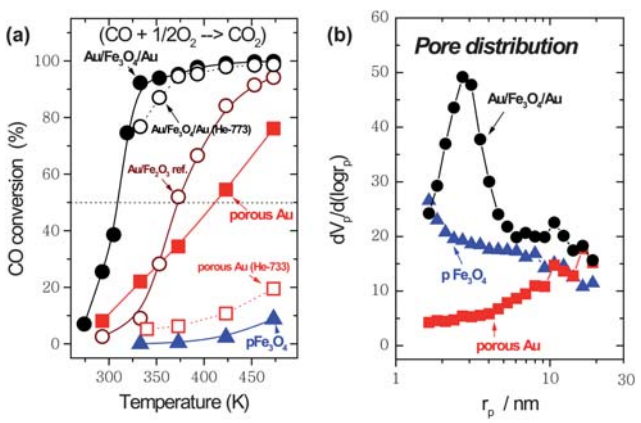

Fig. 3 CO conversion as a function of reaction temperature for CO oxidation (a) and pore distribution (b) for the leached Al-Au-Fe. Those data for leached Al-Au and Al-Fe are also shown for comparison.

energies are in good agreement with the literature (31–35 kJ mol^{-1}).[22,23] Therefore, we do not exclude the contribution of the chemical interaction between Au and Fe_3O_4 at the interface of the Au/Fe_3O_4/Au for the high activity of CO oxidation at present.[22–26] As given in Table 1, the catalytic initial activity with respect to the areal rate (μmol min^{-1} m^{-2} -cat) of the porous Au is similar to that of the nanoporous Au/Fe_3O_4/Au. Pore size distribution, as determined by the BET method shown in Fig. 3 (b), reveals peaks around 3 and 10 nm for the nanoporous Au/Fe_3O_4/Au whereas a very broad distribution around 15 nm is seen for the porous Au. The pore size distribution basically coincides with HRTEM observations, and the high surface area (*ca.* 20 m^2/g) for the nanoporous Au/Fe_3O_4/Au can be attributed to the increase in the fine porosity of Au promoted by the involvement of iron. Therefore, the contribution of iron likely occurs during the leaching process wherein Al_2Fe shows a pinning effect (Fig. S2, ESI†) slowing down the leaching rate on the adjacent Al_2Au phase during dealloying. We expect that lowering the leaching rate would lead to the formation of fine porosity Au. Surprisingly, as shown in Fig. 3 (a), the catalytic initial activity of the nanoporous Au/Fe_3O_4/Au maintained a high CO conversion even after an intentional sintering treatment in a He flow at 773K, whereas the catalytic initial activity for the nanoporous Au drastically decayed due to this treatment. The Fe_3O_4 layers act as barriers preventing the sintering of Au and hence significantly enhanced the thermal stability. For simplicity, we claim that the formation of the lamellar structure of Al_2Au/Al_2Fe/Al_2Au played two major roles at different stages; one was the slowing down of the leaching rate of Al_2Au by Al_2Fe upon leaching and the other was increasing the thermal stability of Fe_3O_4 during the catalytic reaction.

In conclusion, we have developed an alternately layered nanoporous composite which is useful for catalysis and could have two contributions due to each component. The process is simple and practical. First, a ternary $Al_{67}Au_{19}Fe_{14}$ alloy precursor with a fine lamellar structure consisting of Al_2Au and Al_2Fe was prepared by conventional solidification. Second, the resultant lamellar structure was leached with an NaOH solution to form an alternately layered Au/Fe_3O_4/Au dual-porous composite exhibiting high activity and thermal stability. In this study, the involvement of the iron component consequently improved the catalytic activity and thermal stability. If the leached lamellar structure consisted of two elements favored for two different catalytic reactions, namely reaction A and reaction B, and if the combination of reaction A and reaction B was equal to another reaction generally catalyzed by a noble metal such as Pt and Rh, we would be able to use the process described here to intentionally design a composite catalyst to replace the noble metal catalyst. Here we demonstrated the validity of microstructural tailoring using a self-assembled nano-architecture for heterogeneous catalysis based on metallurgy.

Acknowledgements

The authors are grateful to Prof. Osamu Terasaki (Arrhenius Lab. Stockholm University) for fruitful discussions, Mr Eiji Aoyagi (IMR Tohoku University) for TEM observations and Dr Yoshitaka Matsushita and Dr Masahiko Tanaka (NIMS) for help in performing the powder XRD measurements at SPring-8 (beam line 15XU). This work was supported in part by Grant-in-Aid for Scientific Research (A) 19206072 from the Ministry of Education, Culture, Sports, Science and Technology (MEXT).

References

1 M. Stratmann and M. A. Roherder, *Nature*, 2001, **410**, 420.
2 Y. Yamauchi and K. Kuroda, *Chem.–Asian J.*, 2008, **3**, 664.
3 M. S. Wainwright in *Handbook of heterogeneous catalysis*, ed. G. Ertl, H. Knozinger and J. Weitkamp, Wiley-VCH: Weinheim, 1997.
4 H. W. Pickering and C. Wanger, *J. Electrochem. Soc.*, 1967, **114**, 698.
5 M. J. Pryor and J. C. Fisher, *J. Electrochem. Soc.*, 1984, **131**, 1230.
6 A. J. Forty, *Nature*, 1979, **282**, 597.
7 J. Erlebacher, M. J. Aziz, A. Karma, N. Dimitrov and K. Sieradzki, *Nature*, 2001, **410**, 450.
8 V. Zielasek, B. Jürgens, C. Schulz, J. Biener, M. M. Biener, A. V. Hamza and M. Bäumer, *Angew. Chem., Int. Ed.*, 2006, **45**, 8241.
9 C. X. Xu, J. Su, X. Xu, P. Liu, H. Zhao, F. Tian and Y. Ding, *J. Am. Chem. Soc.*, 2007, **129**, 42.
10 T. Fujita, L. H. Qian, K. Inoke, J. Erlebacher and M. W. Chen, *Appl. Phys. Lett.*, 2008, **92**, 251902.
11 A. Wittstock, B. Neumann, A. Schaefer, K. Dumbuya, C. Kubel, M. M. Biener, V. Zielasek, H.-P. Steinruck, J. M. Gottfried, J. Biener, A. Hamza and M. Baumer, *J. Phys. Chem. C*, 2009, **113**, 5593.
12 S. Kameoka and A. P. Tsai, *Catal. Lett.*, 2008, **121**, 337.
13 S. Kameoka and A. P. Tsai, *14th Int. Cong. Catal.*, Seoul, 2008, OC-16.
14 A. Wittstock, V. Zielasek, J. Biener, C. M. Friend and M. Baumer, *Science*, 2010, **327**, 319.
15 M. Tanaka, Y. Katsuya and A. Yamamoto, *Rev. Sci. Instrum.*, 2008, **79**, 075106.
16 R. Elliott, *Eutectic Solidification Processing*, Butterworths, London, 1983.
17 T. B. Massalski,*Binary Alloy Phase Diagrams*, 2nd edn, ASM International, USA, 1990.
18 K. Takanashi, S. Mitani, M. Sano and H. Fujimori, *Appl. Phys. Lett.*, 1995, **67**, 1016.
19 R. Paniago, R. Forrest, P. C. Chow and S. C. Moss, *Phys. Rev. B: Condens. Matter*, 1997, **56**, 13442.
20 J. Gřondilová and M. Rickart, *J. Appl. Phys.*, 2002, **91**, 8246.
21 Gold reference catalysts, *Gold Bull.*, 2003, **36**, 24.
22 M. Haruta, S. Tsubota, T. Kobayashi, H. Kageyama, M. J. Genet and B. Delmon, *J. Catal.*, 1993, **144**, 175.
23 M. J. Kahlich, H. A. Gasteiger and R. J. Behm, *J. Catal.*, 1999, **182**, 430.
24 M. M. Schubert, S. Hackenberg, A. C. van Veen, M. Muhler, V. Plzak and R. J. Behm, *J. Catal.*, 2001, **197**, 113.
25 N. A. Hodge, C. J. Kiely, R. Whyman, M. R. H. Siddiqui, G. J. Hutchings, Q. A. Pankhurst, F. E. Wagner, R. R. Rajaram and S. E. Golunski, *Catal. Today*, 2002, **72**, 133.
26 H. Yin, C. Wang, H. Zhu, S. H. Overbury, S. Sun and S. Dai, *Chem. Commun.*, 2008, 4357.